Rapid Communications

Superconductivity in the van der Waals layered compound PS_2

Yan-Ling Li,[1,*] Elissaios Stavrou,[2] Qiang Zhu,[3] Samantha M. Clarke,[2] Yunguo Li,[1,4] and Hong-Mei Huang[1]

[1]*Laboratory for Quantum Design of Functional Materials, School of Physics and Electronic Engineering, Jiangsu Normal University, Xuzhou 221116, People's Republic of China*

[2]*Lawrence Livermore National Laboratory, Physical and Life Sciences Directorate, Livermore, California 94550, USA*

[3]*Department of Physics and Astronomy, High Pressure Science and Engineering Center, University of Nevada, Las Vegas, Nevada 89154,USA*

[4]*Department of Earth Sciences, UCL, Gower Street, London WC1E 6BT, United Kingdom*

(Received 21 February 2019; revised manuscript received 7 May 2019; published 10 June 2019)

van der Waals (vdW) layered compounds provided a fruitful research platform for the realization of superconductivity. However, a vdW layered superconductor with a high transition temperature (T_c) at ambient conditions is still rare. Here, using variable-composition evolutionary structure predictions, we systematically explored the stable compounds in the P-S system up to 20 GPa. Opposed to the complex stoichiometries at ambient conditions, only one compound, PS_2, is predicted to be thermodynamically stable above 8 GPa. Strikingly, PS_2 is a vdW layered material isostructural to 3*R*-MoS_2 exhibiting a predicted T_c of around 11 K at ambient pressure, both in the bulk and the monolayer form. PS_2 has been successfully synthesized via high-pressure experiments following the theoretical predictions. This enables replacing transition metals with group V elements in transition-metal dichalcogenides and paves the way in the search for vdW layered materials with superior properties.

DOI: 10.1103/PhysRevB.99.220503

vdW layered materials such as graphite, black phosphorus, and transition-metal dichalcogenides (TMDs) have attracted extensive interest due to the weak interlayer interactions that make them easily exfoliable [1–5]. The electronic properties, such as superconductivity, can change dramatically upon reduction from bulk to two dimensions and can effectively be tailored by an external field or charge-carrier doping [3–8]. Recently, superconductivity for the vdW layered compounds has been extensively investigated [4–8]. At ambient pressure conditions, the majority of vdW layered materials are semiconductors while a few of them show metallic or semimetallic behaviors. For semiconducting vdW layered materials, superconductivity can be induced by chemical intercalation, external pressure, and electrostatic gating [9–17]. In the TMD family, there is a strong competition between the charge density wave (CDW) and superconductivity. The transition from a CDW state to superconducting state can be triggered by an external stimulus, as observed in $TiSe_2$ [12], MoS_2 [15], and $MoTe_2$ [14]. Bulk MoS_2 exhibits superconductivity with a T_c of ∼12 K at an ultrahigh pressure of 120 GPa [13]. Thin-film MoS_2 becomes superconducting when it is heavily gated to the conducting regime, in which T_c reaches 10 K at optimal gating [15]. Electrostatically induced superconductivity has also been realized in thin films of 2*H*-WS_2 [16] and 2*H*-$MoSe_2$ [17]. For semimetallic vdW materials, superconductivity has been observed in the Weyl semimetal $MoTe_2$ but with low T_c values (∼0.1 K) under ambient conditions [14]. Upon compression, the T_c of $MoTe_2$ dramatically increases to a maximum value of 8.2 K at 11.7 GPa, accompanied by a 1T'-to-2*H* polytype transformation [14]. Metallic 2*H*-$NbSe_2$, a record holder in intrinsic superconducting TMDs, exhibits a transition temperature of 7.2 K at ambient conditions [18].

Economically, it is also valuable to replace transition metals in TMD materials with more abundant and inexpensive main group elements. Group IVA chalcogenides have attracted great attention because of their emergent physics phenomena such as surface state, quantum spin Hall effects, and superconductivity [19]. $SnSe_2$ has been reported to become superconducting by organometallic intercalation [20], physical gating [19], and external pressure [21]. Recently, Zeng *et al.* induced a superconducting state ($T_c \approx 3.9$ K) in 1*T*-$SnSe_2$ by using the ionic liquid gating technique [19]. It was also reported that 1*T*-$SnSe_2$ exhibits robust superconductivity with a nearly constant $T_c \approx 6.1$ K between 30.1 and 50.3 GPa [21].

In recent years, the search for layered vdW materials that exhibit superconductivity has intensified [6–8]. In this Rapid Communication, we report that phosphorus and sulfur, two neighboring elements in the periodic table, can form an unexpectedly stable layered compound PS_2 under relatively low-pressure conditions. Following this prediction, PS_2 was confirmed by performing high-pressure experiments in a laser-heated diamond anvil cell (LHDAC), starting from an elemental P-S mixture. The synthesized compound was characterized via *in situ* synchrotron x-ray diffraction (XRD) and Raman spectroscopy measurements. PS_2 is predicted to be superconducting with a transition temperature (∼11.3 K) comparable to that (11.5 K) of CaC_6 at ambient pressure [10].

The *ab initio* evolutionary algorithm USPEX [22,23] was used to explore thermodynamically stable P-S compounds and their structures. In these calculations, all stoichiometries were allowed (with the constraint that the total number of atoms in the unit cell is no more than 32 atoms), and calculations

*ylli@jsnu.edu.cn

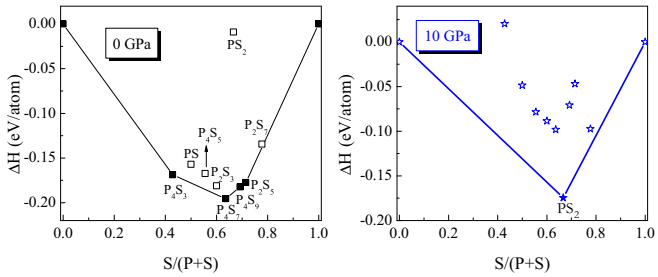

FIG. 1. The predicted convex hull diagrams in a P-S system at pressures of 0 and 10 GPa.

were performed at 1, 5, 10, and 20 GPa, respectively. The pressure-composition phase diagram of the P-S system is shown in Fig. 1 and Supplemental Fig. S1 [24], in which the convex hull was constructed from the normalized formation enthalpies of all the stable structures for each pressure. Thermodynamically, the convex hull at a given pressure connects all stable phases against decomposition into other binaries or elements. We first considered the phase transitions on two ending members (elemental P and S). Phosphorus transforms from the orthorhombic $A17$ structure ($Cmca$) to the rhombohedral $A7$ phase ($R\bar{3}m$) to the simple cubic phase in the pressure range considered [25,26], whereas sulfur in this pressure range undergoes a series of phase transitions from $Fddd$ to $P3_221$ to $R\bar{3}$ and to $I4_1/acd$ [27–29]. Using variable-composition evolutionary searches, we found that the P-S system holds a richer phase diagram at pressures lower than 3 GPa. Four previously reported compounds with discrete cagelike molecules, P_4S_3 [30], P_4S_7 [31], P_4S_9 [32], and P_2S_5 [31] (Supplemental Fig. S2) [24], are thermodynamically stable at zero pressure within a narrow pressure range: P_4S_3 (<2 GPa); P_4S_7 (<6 GPa); P_4S_9 (<1 GPa), and P_2S_5 (<2 GPa). The reported phosphorus polysulfide, P_2S_7 [33] with neutral polymeric strands, is thermodynamically stable one from 1 to 8 GPa. Surprisingly, an unreported compound PS_2 is found to be the only compound thermodynamically stable above 8 GPa as shown in Fig. 1 and Fig. S3 [24]. Below 8 GPa, PS_2 is a metastable compound. We also performed the phonon dispersion curves for PS_2 at a series of pressures (Fig. S4) [24]. The absence of imaginary phonon frequencies confirmed its dynamical stability within the entire range of pressure.

As shown in Fig. 2(a), PS_2 is a layered vdW solid isostructural to $3R$-MoS_2, belonging to the D_{3d} ($R\bar{3}m$) space group [34,35]. Its unit cell is composed of three phosphorus atoms occupying $3a$ Wyckoff sites (0, 0, 0) and six sulfur atoms at $6c$ (0, 0, z). We mention that MoS_2 has two different forms of $3R$ polytypes: One is the $CdCl_2$-type structure (space group $R\bar{3}m$) with inversion symmetry [34,35] which occurs in γ-TaS_2 [35] and β-$TaSe_2$ [35] as well as our PS_2, and another is the $R3m$ structure with broken inversion symmetry which is well known in the TMD family [4,35,36]. Considering that layered TMDs exhibit a variety of polytypes [2–4,14] such as $2H$, $1T$, $1T'$, and T_d, we also examined the possibility of these structures occurred in PS_2. Our density functional theory (DFT) calculations suggested $3R$-MoS_2 with $R\bar{3}m$ symmetry is indeed the ground state among these polytypes [24]. In addition, in order to evaluate the influences of interlayer vdW interaction on structural parameters of PS_2 [24], we considered the versatile vdW density functional proposed by Peng *et al.* (SCAN+rVV10 method) [37], which can produce excellent interlayer spacing and intralayer lattice constants. The calculated lattice parameters are 3.258 Å for a and 17.344 Å for c at ambient conditions, which yields a density of 2.971 g/cm^3 and an interlayer spacing of 5.782 Å. The optimized internal free parameter z is 0.256. PS_2 holds a slightly lower interlayer spacing than that (6.15 Å) of $3R$-MoS_2 [34].

In order to verify the theoretical predictions and explore the pressure range of the stability of PS_2, we performed LHDAC experiments (Fig. S5 [24]) on the phosphorus-sulfur mixture

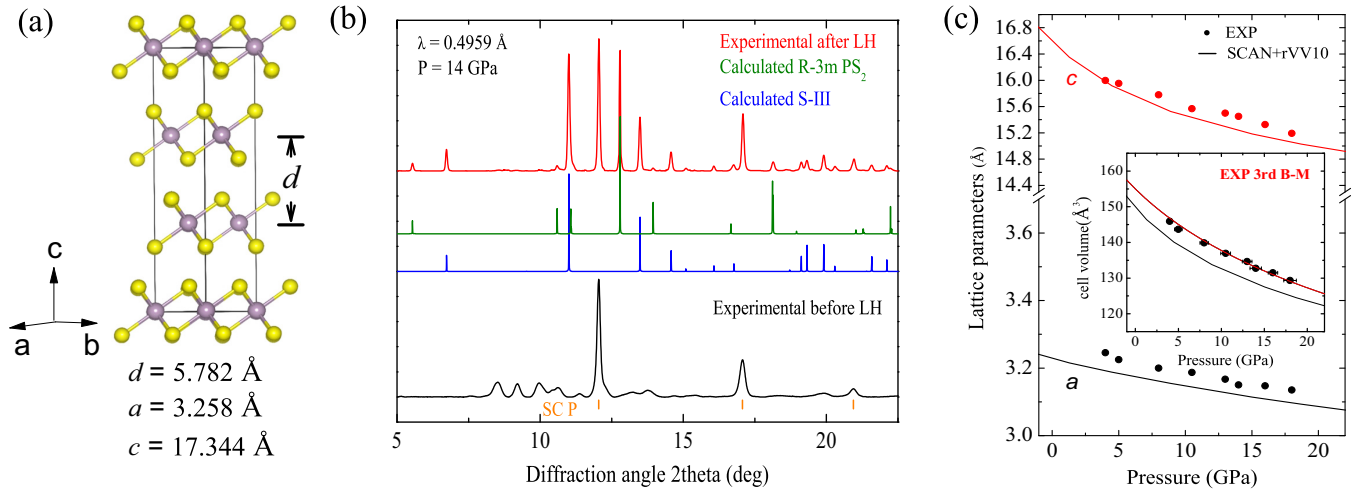

FIG. 2. (a) The crystal structure of the vdW layered compound PS_2. The lattice parameters a and c and interlayer spacing d at zero pressure given. (b) Integrated XRD patterns before laser heating (LH) and after LH to 800 K, respectively. Vertical ticks correspond to expected (assuming continuous Debye rings, see Supplemental Material [24]) positions and intensities of XRD peaks of SC-P, S-III, and PS_2. (c) Pressure dependence of the lattice parameters of PS_2. The inset shows the pressure dependence of the cell volume. Experimental data are shown with solid symbols and theoretical predictions with solid lines. The solid red curve in the inset is the third-order Birch-Murnaghan (3rd BM) equation of states fit to the experimental data.

at various pressures from 10 to 20 GPa and temperatures from 800 to 2000 K. All synthesis experiments concluded the formation of the layered PS_2 compound independently of the starting pressure, the maximum achieved temperature, and the presence or not of thermal insulation (LiF). This observation agrees with the theoretical prediction that the layered PS_2 is the only thermodynamically stable composition above 8 GPa. In Fig. 2(b) we show the XRD patterns ($\lambda = 0.4959$ Å) acquired during a synthesis attempt at 14 GPa. The XRD pattern before LH at room temperature (RT) is representative of a heterogeneous mixture of orthorhombic sulfur (S-I) and simple cubic phosphorous (SC-P). As expected, amorphous red phosphorus converts to the corresponding crystal structures of black phosphorus above 7 GPa [38,39]. The corresponding cell volumes are in excellent agreement with previous high-pressure equation of state (EOS) studies of sulfur and phosphorus [26,28]. New narrow Bragg peaks appear after LH [see Fig. 2(b)], while the Bragg peaks of S-I disappear and the ones of SC-P become narrower due to temperature annealing. The new Bragg peaks can be indexed with a mixture of the predicted PS_2 structure and tetragonal S-III. According to previous studies, at elevated pressure S-I transforms to tetragonal S-III at temperatures below the temperatures achieved by LH in this study and S-III is quenchable at ambient temperature [29]. Bragg peaks of S-III were indexed with $a = 8.423$ Å and $c = 3.521$ Å at 14 GPa, in excellent agreement with Ref. [29]. The remaining Bragg peaks can be indexed with the R-3m-PS_2 with $a = 3.149$ Å and $c = 15.501$ Å, in good agreement with the theoretically predicted values ($a = 3.120$ Å and $c = 15.231$ Å at 14 GPa). A representative Le Bail refinement ($\lambda = 0.3344$ Å) is shown in Supplemental Fig. S6 [24].

With decreasing pressure, the newly synthesized phase remains stable down to 4 GPa, as evidenced from XRD measurements and optical observations. Below this pressure the XRD patterns are representative of a mixture of crystalline P and a disorderedlike (broad Bragg peaks) phase. It is plausible to assume that this disordered phase is the disordered metastable phase of sulfur previously observed on the pressure release of S-III by Degtyareva *et al.* [29]. Thus, we conclude that PS_2 decomposes to P+S below 3 GPa. However, our phonon calculations suggested that PS_2 should be quenchable to the ambient condition. The observed decomposition may be a result of small grain size and large ratio of interfaces, which to some extent reduce the decomposition barrier [40]. Pressure dependence of the lattice parameters and EOS of PS_2 together with the theoretically predicted ones are shown in Fig. 2(c). Experiment and theory agree closely for the lattice parameters and the cell volume. In particular, the experimental and theoretical unit cell volumes differ by less than 4%, which is within the expected accuracy of DFT calculations [41]. We conducted EOS fits to the experimental and calculated PV data using a third-order Birch-Murnaghan EOS and determined the bulk modulus B_0 and the first derivative B_0' [42]. The results of the fits are $V_0 = 152.5(7)$ Å^3, $B_0 = 78.7(15)$ GPa, $B_0' = 4.0(5)$ for the experimental EOS, and $V_0 = 149.5$ Å^3, $B_0 = 56.5$ GPa, $B_0' = 5.9$ for the calculated one.

For PS_2, there are four distinct optical phonon modes at the zone center: two Raman active modes E_g (twofold degeneracy,

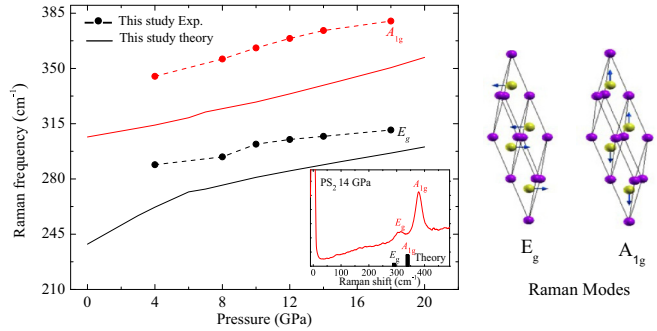

FIG. 3. Frequencies of Raman modes of PS_2 against pressure upon decompression. Experimental results with solid symbols and theoretically predicted with solid lines. The inset shows the experimental Raman spectrum at 14 GPa in comparison with the theoretically predicted Raman modes. Eigenvectors of Raman modes E_g and A_{1g} also given.

S in-plane, basal plane vibrations) and A_{1g} (S out-of-plane, along c-axis vibrations) along with two infrared active modes E_u (twofold degeneracy, in-plane S and P displacements) and A_{2u} (out-of-plane S and P displacements) (see Fig. 3 and Fig. S7 [24]). The Raman spectrum, using the 514.5-nm line of an Ar ion laser for excitation, of the new phase depicted in Fig. 3 shows the presence of two distinct Raman active modes. Relative intensity and frequency separation of the modes allowed us to confidently assign the two modes to the A_{1g} (higher intensity/frequency) and E_g (lower intensity/frequency) of the layered PS_2 compound. Upon pressure release both modes show normal mode behavior (redshift) and can be traced down to 3–4 GPa, in agreement with XRD measurements. Experimental Raman mode frequencies and frequency-pressure slopes are in good agreement with the theoretically calculated ones, given the fact that the generalized gradient approximation (GGA) underestimates the phonon frequencies [43].

The distinctive layered features in PS_2 aroused our intense interest in exploring its electronic properties. Remarkably, PS_2 is predicted to be a phonon-mediated superconductor even at zero pressure. The energy bands of PS_2 at 3 GPa are shown in Fig. 4(a). There is only one energy band crossing the Fermi level along several high-symmetry directions in the Brillouin

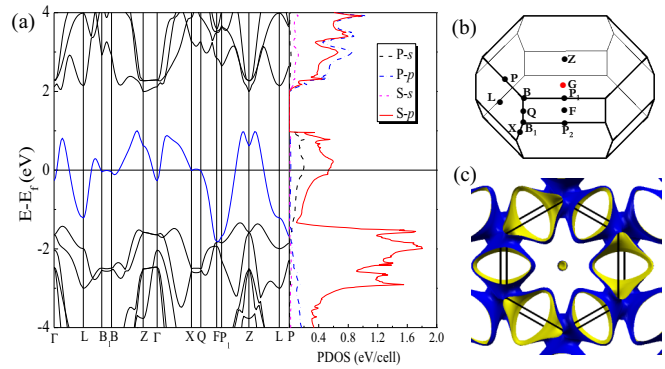

FIG. 4. Energy band, projected electronic density of states (PDOS) (a), Brillouin zone (b), and Fermi surface (c) of PS_2 at 3 GPa. The Fermi level was taken as the energetic reference point.

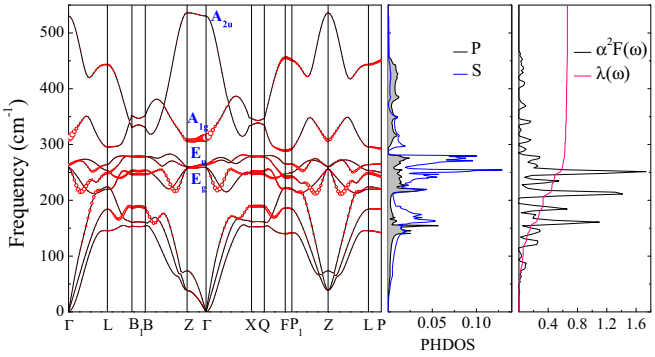

FIG. 5. Phonon spectrum, in which the linewidths for phonon mode $\mathbf{q}\nu$ (i.e., $\gamma_{\mathbf{q}\nu}$) are represented by the area of the red circle, partial atomic phonon DOS, Eliashberg spectral function $\alpha^2F(\omega)$, and integrated $\lambda(\omega)$ for PS_2 at the pressure of 3 GPa.

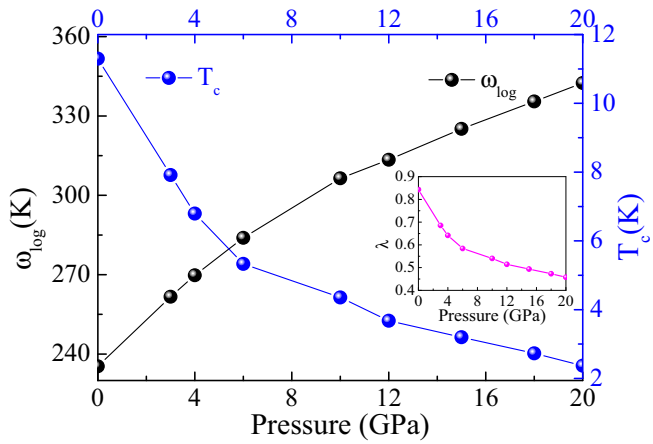

FIG. 6. Calculated T_c values and logarithmic phonon momentum $\omega_{\log}$ vs pressure. The inset shows the integrated electron-phonon coupling λ as a function of pressure.

zone [BZ, see Fig. 4(b)]. The most interesting feature is the presence of nearly flat bands lying right at the Fermi level along the B_1-B and X-Q directions in the BZ. The occurrence of flat and steep slopes near the Fermi level resembles a favorable condition for enhancing Cooper pair formation, which is essential to phonon-mediated superconductivity [44]. The calculated density of states (DOS) shows that there is a strong hybridization between the S-p and P-s electrons in the whole BZ, indicating that these electrons dominate the electronic properties of PS_2. As shown in Fig. 4(c), the Fermi surface (FS) of the PS_2 consists of a small electronlike pocket around Γ point and six linked electron-hole tubes (nearly elliptical sections) with a large surface area running through the BZ borders along the Γ-Z direction, exhibiting an evident 2D behavior. The existence of nearly parallel pieces of the FS is beneficial to the electron-phonon coupling [45]. Both the Fermi pockets and the obvious FS nesting lead to strong electron-phonon interactions in PS_2.

The phonon dispersion curve, partial atomic phonon DOS, Eliashberg spectral function $\alpha^2F(\omega)$, and integrated $\lambda(\omega)$ of PS_2 at 3 GPa are shown in Fig. 5. To gain further insights into the nature of electron-phonon coupling, the linewidths for phonon mode $\mathbf{q}\nu$ (i.e., $\gamma_{\mathbf{q}\nu}$) were attached to phonon dispersion curves. One can identify the contribution to the electron-phonon coupling strength from each phonon mode based on the calculated phonon linewidths. The softening of the E_g branch is observed along the X-Γ-L, B-Z, and P_1-Z-L directions, signaling again strong electron-phonon coupling in PS_2. Such a softening of the mode was previously observed in the superconducting MgB_2 [46]. Combining the calculated phonon linewidths with electronic structure, we conclude that the E_g modes are strongly coupled to electronic bands from S-p_x and S-p_y as well as P-s states since E_g modes involve atomic displacements in the x-y plane. The deltalike peak around 251 cm^{-1} in both the spectral function $\alpha^2F(\omega)$ and phonon DOS originates mostly from the E_g modes with calculated energies in the ranges of 207–257 cm^{-1}, which contributes to 33.3% of the total λ value. The A_{1g} branch possesses energies in the ranges of 292–371 cm^{-1} and holds the highest phonon linewidth around the Γ point. However, it contributes to only 3.1% of the total λ value because of the strong anisotropy of the linewidth of the A_{1g} branch in the BZ. These results indicate that the sulfur atoms dominate superconductivity in PS_2, due to the prominent contributions to the electron-phonon interaction. Phonons from the sulfur atoms together with the electrons from the S-p and P-s states provide the strong electron-phonon coupling indispensable for superconductivity in PS_2.

From the value of λ, one can estimate the T_c using the Allen and Dynes formula [47]. Taking a typical value of 0.11 for μ^* along with the calculated $\omega_{\log}$ of 235 cm^{-1}, we obtained a T_c of 11.3 K for PS_2 at zero pressure. The changes of λ, $\omega_{\log}$, and T_c with increasing pressure in PS_2 are depicted in Fig. 6. Applying pressure on PS_2 clearly leads to a significant decrease of λ and T_c. At 20 GPa, T_c is only 2.4 K. The sharp drop of λ is closely associated with the decrease of DOS at the Fermi level because the Fermi level moves up as the pressure increases.

The single- or few-layered-thick, two-dimensional (2D) crystals are particularly interesting due to their potential use in low-dimensional electronics [2,5,8]. Therefore, it is interesting to discuss the superconductivity of the monolayer PS_2. Compared with bulk superconductors, 2D superconductors are more convenient for fabrication in modern electronic applications. So far, the well-defined 2D intrinsic superconductors were rarely reported. For TMDs, only monolayer 2H-$NbSe_2$ [48] was found to exhibit intrinsic superconductivity with a relatively lower transition temperature (below 3 K) than that of its bulk counterpart (7.2 K) [18,49,50]. The weakened superconductivity due to the reduction of the dimensionality is a universal behavior in the TMD family except for TaS_2 [51]. For our PS_2, the superconductivity also persisted from bulk to monolayer. Different from the $NbSe_2$, we surprisingly found that at ambient pressure the monolayer PS_2 has a slightly lower T_c (about 10.8 K) than bulk because of a slightly lower coupling constant (about 0.8) than bulk, indicating that bulk PS_2 could be a 2D superconductor.

In conclusion, we report a layered PS_2 compound from a joint effort between theory and experiment. Our complete survey on the pressure-composition phase diagram for the P-S system at pressures up to 20 GPa yielded a compound PS_2 to become thermodynamically stable above 8 GPa. PS_2

is predicted to be an unusual example of a superconducting vdW layered material, exhibiting superconductivity with an unexpectedly high transition temperature (∼11.3 K) at ambient conditions. Monolayer PS_2 retains the superconducting property of bulk PS_2, suggesting that PS_2 is an ideal candidate material for exploring 2D superconductivity. Experimental results, from diffraction and spectroscopic techniques, unambiguously identified the synthesized compounds as the predicted layered $R\bar{3}m$-PS_2. We believe the discovery of a nonintuitive vdW layered compound between group V and VI elements will open an avenue in vdW layered material design.

We acknowledge support from the National Natural Science Foundation of China (Grant No. 11674131) and the 333 project of Jiangsu province. Part of this work was performed under the auspices of the U.S. Department of Energy by Lawrence Livermore National Security, LLC under Contract No. DE-AC52-07NA27344. We gratefully acknowledge the LLNL LDRD program for funding support of this project under 18-LW-036. Part of this work was performed at GeoSoilEnviroCARS (The University of Chicago, Sector 13), Advanced Photon Source (APS), Argonne National Laboratory. GeoSoilEnviroCARS is supported by the National Science Foundation-Earth Sciences (EAR-1634415) and Department of Energy-GeoSciences (DE-FG02-94ER14466). This research used resources of the Advanced Photon Source, a U.S. Department of Energy (DOE) Office of Science User Facility operated for the DOE Office of Science by Argonne National Laboratory under Contract No. DE-AC02-06CH11357. The ALS is supported by the Director, Office of Science, BES of DOE under Contracts No. DE-AC02-05CH11231 and No. DE-AC02-06CH11357. Beamline 12.2.2 at the Advanced Light Source is a DOE Office of Science User Facility under Contract No. DE-AC02-05CH11231.

Y.L.L. and E.S. contributed equally to this work.

[1] X. Qiu and W. Ji, Illuminating interlayer interactions, Nat. Mater. **17**, 211 (2018).

[2] A. V. Kolobov and J. Tominaga, *Two-Dimensional Transition-Metal Dichalcogenides* (Springer, Berlin, 2016).

[3] H. Yang, S. Kim, M. Chhowalla, and Y. Lee, Structural and quantum-state phase transition in van der Waals layered materials, Nat. Phys. **13**, 931 (2017).

[4] G. H. Han, D. L. Duong, D. H. Keum, S. J. Yun, and Y. H. Lee, van der Waals metallic transition metal dichalcogenides, Chem. Rev. **118**, 6297 (2018).

[5] S. Manzeli, D. Ovchinnikov, D. Pasquier, O. V. Yazyev, and A. Kis, 2D transition metal dichalcogenides, Nat. Rev. Mater. **2**, 15. 17033 (2017).

[6] R. P. Smith, T. E. Weller, C. A. Howard, M. P. Dean, K. C. Rahnejat, S. S. Saxena, and M. Ellerby, Superconductivity in graphite intercalation compounds, Physica C **514**, 50 (2015).

[7] R. A. Klemm, Pristine and intercalated transition metal dichalcogenide superconductors, Physica C **514**, 86 (2015).

[8] Y. Saito, T. Nojima, and Y. Iwasa, Highly crystalline 2D superconductors, Nat. Rev. Mater. **2**, 16094 (2016).

[9] G. Csányi, P. B. Littlewood, A. H. Nevidomskyy, C. J. Pickard, and B. D. Simons, The role of the interlayer state in the electronic structure of superconducting graphite intercalated compounds, Nat. Phys. **1**, 42 (2005).

[10] N. Emery, C. Hérold, M. d'Astuto, V. Garcia, C. Bellin, J. F. Marêché, P. Lagrange, and G. Loupias, Superconductivity of Bulk CaC_6, Phys. Rev. Lett. **95**, 087003 (2005).

[11] A. Gauzzi, S. Takashima, N. Takeshita, C. Terakura, H. Takagi, N. Emery, C. Hérold, P. Lagrange, and G. Loupias, Enhancement of Superconductivity and Evidence of Structural Instability in Intercalated Graphite CaC_6 Under High Pressure, Phys. Rev. Lett. **98**, 067002 (2007).

[12] E. Morosan, H. W. Zandbergen, B. S. Dennis, J. W. G. Bos, Y. Onose, T. Klimczuk, A. P. Ramirez, N. P. Ong, and R. J. Cava, Superconductivity in Cu_xTiSe_2, Nat. Phys. **2**, 544 (2006).

[13] Z. Chi, X. Chen, F. Yen, F. Peng, Y. Zhou, J. Zhu, Y. Zhang, X. Liu, C. Lin, S. Chu, Y. Li, J. Zhao, T. Kagayama, Y. Ma, and Z. Yang, Superconductivity in Pristine $2H_a$-MoS_2 at Ultrahigh Pressure, Phys. Rev. Lett. **120**, 037002 (2018).

[14] Y. Qi *et al.*, Superconductivity in Weyl semimetal candidate $MoTe_2$, Nat. Commun. **7**, 11038 (2016).

[15] J. T. Ye, Y. J. Zhang, R. Akashi, M. S. Bahramy, R. Arita, and Y. Iwasa, Superconducting dome in a gate-tuned band insulator, Science **338**, 1193 (2012).

[16] S. Jo, D. Costanzo, H. Berger, and A. F. Morpurgo, Electrostatically induced superconductivity at the surface of WS_2, Nano Lett. **15**, 1197 (2015).

[17] W. Shi, J. Ye, Y. Zhang, R. Suzuki, M. Yoshida, J. Miyazaki, N. Inoue, Y. Saito, and Y. Iwasa, Superconductivity series in transition metal dichalcogenides by ionic gating, Sci. Rep. **5**, 12534 (2015).

[18] T. Yokoya, T. Kiss, A. Chainani, S. Shin, M. Nohara, and H. Takagi, Fermi surface sheet-dependent superconductivity in $2H$-$NbSe_2$, Science **294**, 2518 (2001).

[19] J. Zeng *et al.*, Gate-induced interfacial superconductivity in $1T$-$SnSe_2$, Nano Lett. **18**, 1410 (2018).

[20] D. O'Hare, H.-V. Wong, S. Hazell, and J. W. Hodby, Relatively isotropic superconductivity at 8.3 K in the lamellar organometallic intercalate $SnSe_2\{Co(\eta\text{-}C_5\ H_5)_2\}_{0.3}$, Adv. Mater. **4**, 658 (1992).

[21] Y. Zhou *et al.*, Pressure-induced metallization and robust superconductivity in pristine $1T$-$SnSe_2$, Adv. Electron. Mater. **4**, 1800155 (2018).

[22] A. R. Oganov and C. W. Glass, Crystal structure prediction using *ab initio* evolutionary techniques: Principles and applications, J. Chem. Phys. **124**, 244704 (2006).

[23] A. O. Lyakhov, A. R. Oganov, H. T. Stokes, and Q. Zhu, New developments in evolutionary structure prediction algorithm USPEX, Comput. Phys. Commun. **184**, 1172 (2013).

[24] See Supplemental Material at http://link.aps.org/supplemental/10.1103/PhysRevB.99.220503 for a detailed description of theoretical calculations and experimental methods, convex hull, crystal structures, phonon spectrum, Le Bail refinement, XRD patterns, structural parameters of PS_2 using different vdW corrections, and Supplemental Figs. S1–S7, which includes Refs. [52–65].

[25] J. C. Jamieson, Crystal structures adopted by black phosphorus at high pressures, Science **139**, 1291 (1963).

[26] T. Kikegawa and H. Iwasaki, An X-ray diffraction study of lattice compression and phase transition of crystalline phosphorus, Acta Crystallogr., Sect. B: Struct. Sci. **39**, 158 (1983).

[27] J. Donohue, A. Caron, and E. Goldish, The crystal and molecular structure of S_6 (sulfur-6), J. Am. Chem. Soc. **83**, 3748 (1961).

[28] Y. Akahama, M. Kobayashi, and H. Kawamura, Pressure-induced structural phase transition in sulfur at 83 GPa, Phys. Rev. B **48**, 6862 (1993).

[29] O. Degtyareva, E. Gregoryanz, M. Somayazulu, P. Dera, H.-k. Mao, and R. J. Hemley, Novel chain structures in group VI elements, Nat. Mater. **4**, 152 (2005).

[30] G. R. Burns, J. R. Rollo, and R. W. Syme, Raman spectra of single crystals of α-P_4S_3, J. Raman Spectrosc. **19**, 345 (1988).

[31] A. Vos, R. Olthof, F. Van Bolhuis, and R. Botterweg, Refinement of the crystal structures of some phosphorus sulphides, Acta Crystallogr. **19**, 864 (1965).

[32] W. Hilmer, Die struktur eines phosphor (III,V)-sulfids der ungefähren zusammensetzung P_4S_9, Acta Crystallogr., Sect. B: Struct. Sci. **25**, 1229 (1969).

[33] T. Rödl, R. Weihrich, J. Wack, J. Senker, and A. Pfitzner, Rational syntheses and structural characterization of sulfur-rich phosphorus polysulfides: α-P_2S_7 and β-P_2S_7, Angew. Chem., Int. Ed. **50**, 10996 (2011).

[34] R. E. Bell and R. E. Herfert, Preparation and characterization of a new crystalline form of molybdenum disulfide, J. Am. Chem. Soc. **79**, 3351 (1957).

[35] *Crystallography and Crystal Chemistry of Materials with Layered Structures*, edited by F. Lévy (Reidel, Dordrecht, 1976).

[36] R. Suzuki *et al.*, Valley-dependent spin polarization in bulk MoS_2 with broken inversion symmetry, Nat. Nanotechnol. **9**, 611 (2014).

[37] H. Peng, Z.-H. Yang, J. P. Perdew, and J. Sun, Versatile Van Der Waals Density Functional Based on a Meta-Generalized Gradient Approximation, Phys. Rev. X **6**, 041005 (2016).

[38] J. M. Zaug, A. K. Soper, and S. M. Clark, Pressure-dependent structures of amorphous red phosphorus and the origin of the first sharp diffraction peaks, Nat. Mater. **7**, 890899 (2008).

[39] E. Rissi, E. Soignard, K. McKiernan, C. Benmore, and J. Yarger, Pressure-induced crystallization of amorphous red phosphorus, Solid State Commun. **152**, 390 (2012).

[40] R. Liu, T. Zhang, L. Yang, and Z. Zhou, Effect of particle size on thermal decomposition of alkali metal picrates, Thermochim. Acta **583**, 78 (2014).

[41] Y. L. Li, S. N. Wang, A. R. Oganov, H. Gou, J. S. Smith, and T. A. Strobel, Investigation of exotic stable calcium carbides using theory and experiment, Nat. Commun. **6**, 6974 (2015).

[42] F. Birch, Finite strain isotherm and velocities for single-crystal and polycrystalline NaCl at high pressures and 300 K, J. Geophys. Res. **83**, 1257 (1978).

[43] F. Favot and A. Dal Corso, Phonon dispersions: Performance of the generalized gradient approximation, Phys. Rev. B **60**, 11427 (1999).

[44] Y. L. Li, W. Luo, Z. Zeng, H. Q. Lin, H. k. Mao, and R. Ahuja, Pressure-induced superconductivity in CaC_2, Proc. Natl. Acad. Sci. USA **110**, 9289 (2013).

[45] Y. L. Li, W. Luo, X. J. Chen, Z. Zeng, H. Q. Lin, and R. Ahuja, Formation of nanofoam carbon and re-emergence of superconductivity in compressed CaC_6, Sci. Rep. **3**, 3331 (2013).

[46] A. Q. R. Baron, H. Uchiyama, Y. Tanaka, S. Tsutsui, D. Ishikawa, S. Lee, R. Heid, K.-P. Bohnen, S. Tajima, and T. Ishikawa, Kohn Anomaly in MgB_2 by Inelastic X-Ray Scattering, Phys. Rev. Lett. **92**, 197004 (2004).

[47] P. B. Allen and R. Dynes, Transition temperature of strong-coupled superconductors reanalyzed, Phys. Rev. B **12**, 905 (1975).

[48] M. Ugeda *et al.*, Characterization of collective ground states in single-layer $NbSe_2$, Nat. Phys. **12**, 92 (2016).

[49] X. Xi, Z. Wang, W. Zhao, J. Park, K. Law, H. Berger, L. Forró, J. Shan, and K. Mak, Ising pairing in superconducting $NbSe_2$ atomic layers, Nat. Phys. **12**, 139 (2016).

[50] H. Wang *et al.*, High-quality monolayer superconductor $NbSe_2$ grown by chemical vapour deposition, Nat. Commun. **8**, 394 (2017).

[51] E. Navarro-Moratalla *et al.*, Enhanced superconductivity in atomically thin TaS_2, Nat. Commun. **7**, 11043 (2016).

[52] J. Hafner, Materials simulations using VASP—a quantum perspective to materials science, Comput. Phys. Commun. **177**, 6 (2007).

[53] J. P. Perdew, K. Burke, and M. Ernzerhof, Generalized Gradient Approximation Made Simple, Phys. Rev. Lett. **77**, 3865 (1996).

[54] G. Kresse and D. Joubert, From ultrasoft pseudopotentials to the projector augmented-wave method, Phys. Rev. B **59**, 1758 (1999).

[55] P. Giannozzi *et al.*, Advanced capabilities for materials modelling with QUANTUM ESPRESSO, J. Phys.: Condens. Matter **29**, 465901 (2017).

[56] K. Syassen, Ruby under pressure, High Press. Res. **28**, 75 (2008).

[57] M. Matsui, High temperature and high pressure equation of state of gold, J. Phys.: Conf. Ser. **215**, 012197 (2010).

[58] V. B. Prakapenka, A. Kubo, A. Kuznetsov, A. Laskin, O. Shkurikhin, P. Dera, M. L. Rivers, and S. R. Sutton, Advanced flat top laser heating system for high pressure research at GSECARS: Application to the melting behavior of germanium, High Press. Res. **28**, 225 (2008).

[59] M. Kunz *et al.*, A beamline for high-pressure studies at the advanced light source with a superconducting bending magnet as the source, J. Synchrotron Radiat. **12**, 650 (2005).

[60] C. Prescher and V. B. Prakapenka, DIOPTAS: A program for reduction of two-dimensional x-ray diffraction data and data exploration, High Press. Res. **35**, 223 (2015).

[61] W. Kraus and G. Nolze, POWDER CELL—a program for the representation and manipulation of crystal structures and calculation of the resulting x-ray powder patterns, J. Appl. Crystallogr. **29**, 301 (1996).

[62] B. H. Toby and R. B. Von Dreele, GSAS-II: The genesis of a modern open-source all purpose crystallography software package, J. Appl. Crystallogr. **46**, 544 (2013).

[63] V. V. Struzhkin, D. Y. Kim, E. Stavrou, T. Muramatsu, H.-k. Mao, C. J. Pickard, R. J. Needs, V. B. Prakapenka, and A. F. Goncharov, Synthesis of sodium polyhydrides at high pressures, Nat. Commun. **7**, 12267 (2016).

[64] A. Boultif and D. Louër, Powder pattern indexing with the dichotomy method, J. Appl. Crystallogr. **37**, 724 (2004).

[65] E. Stavrou, A. Muhtar, F. M. Mohammad, and A. F. Goncharov, Probing the different spatial scales of Kel F-800 polymeric glass under pressure, Sci. Rep. **3**, 1290 (2013).